CERN 94-05
13 October 1994

CERN 94-05

ORGANISATION EUROPÉENNE POUR LA RECHERCHE NUCLÉAIRE
CERN EUROPEAN ORGANIZATION FOR NUCLEAR RESEARCH

CAS CERN ACCELERATOR SCHOOL

Ninth John Adams Memorial Lecture

CRYSTAL CHANNELING
or
HOW TO BUILD A "1000 TESLA MAGNET"

Lecture delivered at CERN on 23 November 1993

Søren Pape Møller
Institute for Synchrotron Radiation
Aarhus University
Denmark

GENEVA
1994

ISSN 0007-8328
ISBN 92-9083-064-6

CERN 94-05
13 October 1994

ORGANISATION EUROPÉENNE POUR LA RECHERCHE NUCLÉAIRE
CERN EUROPEAN ORGANIZATION FOR NUCLEAR RESEARCH

CAS CERN ACCELERATOR SCHOOL

Ninth John Adams Memorial Lecture

CRYSTAL CHANNELING
or
HOW TO BUILD A "1000 TESLA MAGNET"

Lecture delivered at CERN on 23 November 1993

Søren Pape Møller
Institute for Synchrotron Radiation
Aarhus University
Denmark

GENEVA
1994

CERN–Service d'information scientifique–RD/931–1600–octobre 1994

ABSTRACT

When charged particles pass through a crystal along a crystallographic direction, the coherent scattering on the lattice atoms forces the particles to follow the lattice direction. The transmission through an aligned crystal is very different from the passage through an amorphous foil, and drastically changes the interaction with the crystal atoms. This channeling effect has many applications at low energy within both fundamental and applied physics. Also when the crystal is bent, the particles will follow the crystallographic direction. In this way, a crystal can deflect a high-energy beam corresponding to a magnetic field around 1000 Tesla, although with some losses. The lecture will be biased towards high energies (> 1 GeV), and experimental results from several investigations of the channeling effect at high energy will be shown. In particular, results from recent bending and extraction experiments will be presented.

Plate 1 A 4 cm-long silicon crystal has a bending power of more than 10 tesla-metres, normally requiring a conventional bending magnet about six metres long, such as the one in the background.

CONTENTS

1. INTRODUCTION

1.1 Channeling at CERN

The experimental investigations of the channeling effect started at CERN around the time when the SPS was built under the leadership of John Adams and continued during the period 1976-1980 when CERN was directed by John Adams (and Leon van Hove). The initiation of these studies was partly due to the invention of drift and multi-wire chambers by George Charpak at CERN, which made measurements of the very small channeling angles at high energy possible. Other persons of importance to the start-up of this programme are Karl Ove Nielsen and Erik Uggerhøj from Aarhus, of which the latter has led these studies up to the present time. High-energy channeling has also been studied in the USA and in Russia.

The first observations of the channeling effect at CERN was made at the PS with 1.2 GeV/c protons starting in 1974 and the first results were published shortly after [1]. Since then, these channeling studies have been performed at CERN both at the PS and SPS, and also by other groups at ISOLDE.

The present lecture is to a large extent based on a lecture given at the course on Advanced Accelerator Physics held by the CERN Accelerator School on Rhodes Island, Greece, 20 September to 1 October 1993, and published in the proceedings from this course. Only Section 4, manifestations of channeling, has been appreciably enlarged.

1.2 Introductlon to Channeling

A crystal is a regular arrangement of atoms sitting on so-called lattice positions. Looking on a crystal with a magnifying glass, certain directions look open, and the crystal atoms appear to be arranged as pearls on strings or planes, see Fig. 1 a). Intuitively, the transmission of charged particles along such directions will be very different from the passage through an amorphous foil, or along a non-aligned direction; so-called 'random' direction. As we will see in Section 2, the motion along such channeling directions is mainly governed by coherent scatterings on strings or planes of atoms, and not by the individual scatterings on single atoms. It is these strings or planes that give rise to immense electric fields over macroscopic distances; i.e. the crystal thickness.

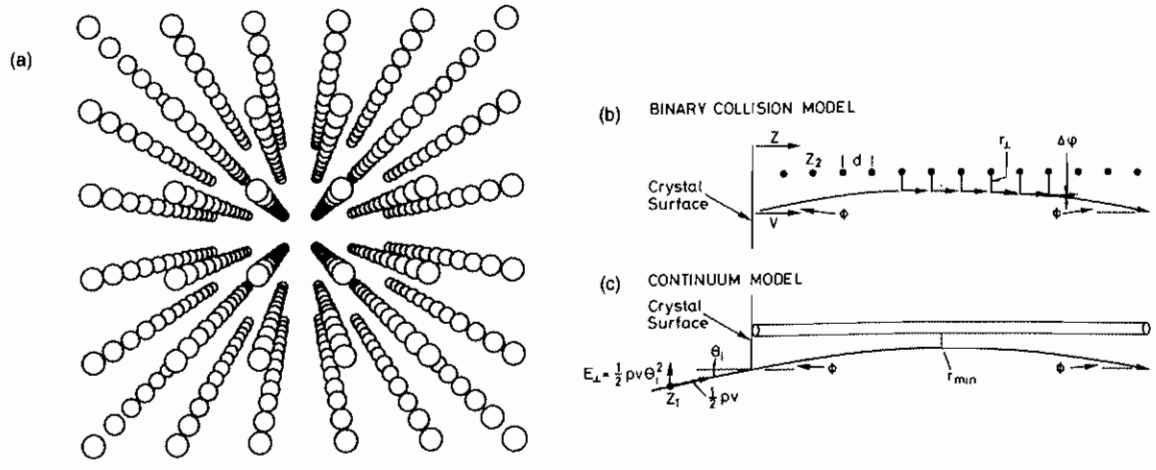

Fig.1 a) Perspective view of simple crystalline structure. b) and c) Schematic drawing of a trajectory in the binary and continuum model.

The channeling effect was discovered in the early sixties by the anomalous energy loss of positive ions in crystalline materials [2,3,4]. A comprehensive theoretical treatment was

soon given by Lindhard [5] and this work has been the basis for all subsequent work. Actually, already in 1912 Stark [6] had predicted: "In Kristallen werden demnach elektromagnetisch empfindliche Teilchen längs ausgezeichneten Achsen viele größere Schichtdicken zu durchdringen vermögen als in amorphen Körpern. .... Es wird demnach in einem Kristall nicht bloβ die Absorption, sondern auch die Zerstreuung von Strahlenteilchen selektiv in verschiedenen Achsen erfolgen." The influence of the channeling effect on the penetration of charged particles through crystals has since been studied by a variety of methods, and the applications of the effect are widespread within both fundamental and applied physics. In particular the applications within semiconductor and ion implantation technology are important.

A new development started in the mid-seventies, when the investigations at high energy began [1]. One motivation was the possibility to use heavy particles of both positive and negative charge, e.g. π^+ and π^-, as a complement to the investigations at low energy with electrons and positrons. The basic interest in channeling was further revived at both low and high energy by the prediction [7,8] and experimental verification [9,10] of channeling radiation, i.e. the electromagnetic radiation emitted by channeled electrons and positrons.

Another development, of prime interest in the present article, was the prediction [11] and observation [12,13] of beam bending by transmission of charged particles through bent crystals.

The present lecture will give an introduction to channeling with emphasis on qualitative aspects and physical insight. Some essential formulae will be given, and it is the hope that the reader after this lecture will be able to evaluate important quantities. Furthermore, we will confine ourselves to high energies (> 1 GeV) and mainly discuss the applications of channeling in beam bending and extraction, the techniques relying on channeling which are presently feasible. We shall also mainly discuss particles of positive charge, and implicitly assume the projectiles to be protons moving with a velocity close to the velocity of light, unless otherwise explicitly stated.

2. CHANNELING IN A CRYSTAL

2.1 Applicability of Classical Mechanics

Let us at this point make a small digression, since it is not at all clear how to describe the transmission of the projectile through the crystal. As was first discussed by Bohr [14], the quantity for determining whether one can apply classical mechanics for an orbital description of scattering in a Coulomb field is $\kappa \equiv 2Z_1Z_2e^2/hv$. Here Z_1 and Z_2 are the projectile and target atomic numbers and v is the projectile velocity. For $\kappa > 1$ the classical picture is a good approximation. As is easily seen, for fast particles this Bohr condition is not fullfilled. This condition is even more restrictive, when screening from the atomic electrons is taken into account. Hence it may appear surprising, that channeling can be described by classical mechanics if the projectile mass is large compared to the electron rest mass [5]. Qualitatively, one may argue that in a collision with a string of atoms it is the charge of all the nuclei in the string participating in the collision that should be inserted in the Bohr condition. Strictly, one may derive a 'transverse Bohr condition', $\kappa_\perp \equiv [(\gamma M/m)Z_1Z_2^{1/3}a_0/d]^{1/2} \gg 1$, for classical mechanics to apply in the so-called transverse plane. Here $\gamma \equiv (1-v^2/c^2)^{-1/2}$, M and m the particle and electron rest mass, $a_0 \equiv h^2/me^2 = 0.511$ Å the Bohr radius and d the atom spacing. As is easily seen, this condition is fullfilled for heavy particles, but maybe more surprisingly also for electrons/positrons with large relativistic mass.

2.2 The Continuum Approximation

For charged particles incident on a crystal with a small angle to an axial direction,

there is a strong correlation between the successive collisions with the string atoms. In other words, the impact parameter changes slowly between subsequent binary collisions, see Fig. 1. This led Lindhard [5] to the introduction of the continuum model, in which the atomic string is replaced by a continuum string obtained by smearing the atomic charges along the string. The channeling picture is now based on a separation between the longitudinal motion along the crystalline direction and the transverse motion, since the interaction between the projectile and the continuum string is independent of the longitudinal coordinate z.

This continuum approximation, outlined above for the atomic string, can also be used when a particle is incident on a crystal with a small angle to a plane of atoms. In this case the atomic charges are smeared over the plane. The transverse motion is two dimensional for the axial case and one dimensional for the planar case, and it is this transverse motion which describes the motion of channeled particles.

The interaction between the projectile and the string or plane is described by continuum potentials. The string potential is obtained by averaging the atomic potential $V(r)$ along the string, i.e.

$$U(\vec{r}_\perp) = \frac{1}{d}\int_{-\infty}^{\infty} V(\vec{r}_\perp, z)\, dz \tag{1}$$

where $r_\perp$ is the coordinate in the plane perpendicular to the string, i.e. the *transverse plane*. Correspondingly, in the planar case the planar continuum potential takes the form

$$Y(y) = Nd_p \int V(\sqrt{x^2+y^2+z^2})\, dx dz \tag{2}$$

where N is the atomic density, d_p the planar spacing, and y the transverse coordinate.

In this continuum model the so-called *transverse energy* $E_\perp$ is a conserved quantity, since the potential is independent of the longitudinal coordinates, z and x,z in the axial and planar cases, respectively. This transverse energy is to a very good approximation given by

$$E_\perp = \frac{p_\perp^2}{2\gamma M} + U(\vec{r}_\perp) = \tfrac{1}{2} pv\psi^2 + U(\vec{r}_\perp) \tag{3}$$

where the first term is the kinetic energy and the second the potential energy. Here p is the momentum of the particle and ψ the local angle to the string/plane direction. In the continuum approximation, the transverse energy of a given particle is given by its initial value, i.e. the value it acquired at the surface of the crystal,

$$E_\perp = E_\perp(z=0) = \tfrac{1}{2} pv\psi_0^2 + U(r_{\perp 0})\,. \tag{4}$$

This also means that even for a parallel beam perfectly aligned with the crystalline direction, there will be a distribution in transverse energy; an effect called *surface transmission*. In Fig. 2 are shown the single-string potential for the <100> string in Ge at room temperature, and examples of trajectories in the transverse plane of three particles with different transverse energies.

Previously, we have implicitly assumed the projectile to have a positive charge. Negative particles may also be channeled, and the main change in the above picture is a change of sign in the potentials, which means that contrary to positive particles which are repelled from the strings and planes, negative particles are focused around the strings and planes of atoms.

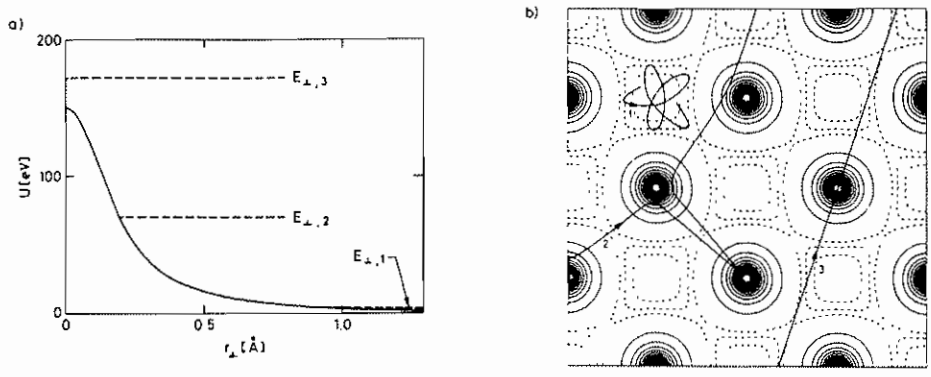

Fig. 2 a) Single-string potential. b) Motion in transverse plane.

2.3 Critical Angles

An important quantity, directly observable, is the *critical channeling angle*. This is defined here as the angle of incidence which allows the particle to penetrate into the string or plane. Hence it can be found by equating the transverse kinetic energy to the maximum potential height,

$$E_\perp^{crit} = \tfrac{1}{2} pv\psi_{crit}^2 = U^{\max}. \tag{5}$$

The critical angle is approximately given by the Lindhard critical angles ψ_1 and ψ_p for the axial and planar case respectively,

$$\psi_1 = \sqrt{\frac{4Z_1Z_2e^2}{pvd}}\ , \qquad \psi_p = \sqrt{4Z_1Z_2e^2Nd_pCa/pv}\ . \tag{6}$$

In the formula for the planar angle, $C \approx \sqrt{3}$ is a constant and $a = 0.8853a_0(Z_1^{2/3}+Z_2^{2/3})^{-1/2}$ a screening length. For the <111> axial and (110) planar direction in silicon, we have

$$\psi_1 = 15\mu\text{rad}/\sqrt{p[\text{TeV/c}]}\ , \qquad \psi_p = 5\mu\text{rad}/\sqrt{p[\text{TeV/c}]}\ . \tag{7}$$

Particles with $E_\perp < E_\perp^{crit}$ are said to be *channeled*, and these particles will, in first approximation, stay channeled. Particles with $E_\perp >> E_\perp^{crit}$ are called *random* particles and are moving through the crystal as if the target was amorphous.

In Fig. 3 are shown calculated surface-transmission probabilities, i.e. the fraction of the beam initially channeled, for 450 GeV protons in silicon at room temperature using the so-called Doyle-Turner potential, see below. The surface transmission is calculated as function of beam divergence for incidence parallel to the (110), (100) and (111) planes.

2.4 Thermal Vibrations

Up to this point we have implicitly assumed that the lattice atoms were static. In reality, they are vibrating around their mean position with a temperature-dependent vibration

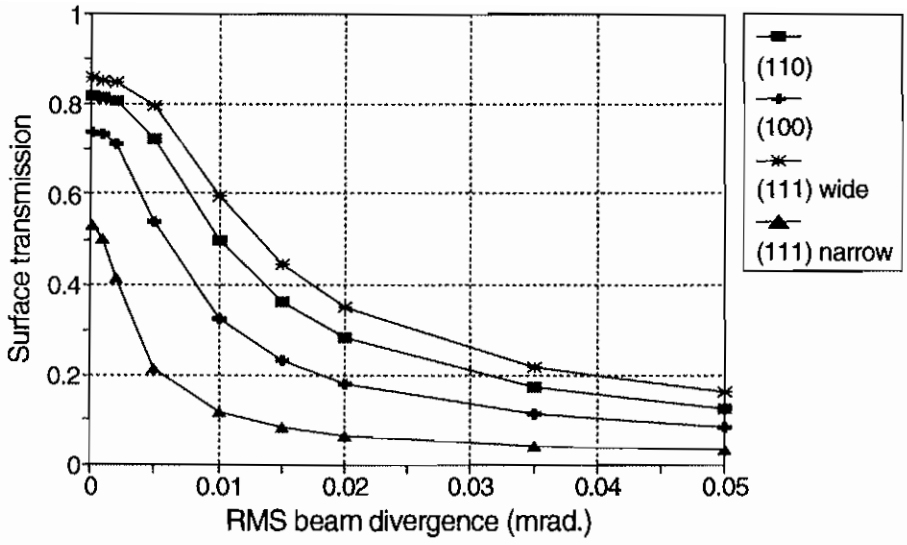

Fig. 3 Calculated surface transmission for a 450-GeV proton beam in a silicon crystal

amplitude ρ. In silicon the one-dimensional rms thermal displacement is $\rho_1 = 0.075$ Å at 300 K, to be compared to the lattice constant a = 5.431 Å. The uncertainty in position owing to these thermal vibrations gives rise to a transverse smearing, and the resulting 'thermally averaged' continuum string potential is given by

$$U_T(\vec{r}_\perp) = \int P(\vec{r}_\perp) U(\vec{r}_\perp - \vec{r}_\perp) d^2\vec{r}_\perp' \,. \tag{8}$$

The probability distribution P of the target atoms is gaussian, that is

$$P(\vec{r}_\perp) = (\pi\rho^2)^{-1} \exp(-r_\perp^2/\rho^2) \tag{9}$$

where ρ^2 is the two-dimensional mean-square thermal displacement from the string. Qualitatively, the main effect of the thermal vibrations occurs at small distances from the string, where the infinite static potential is modified to have a finite maximum. A similar thermal smearing applies for the planar potential, but the influence of the thermal vibrations is here rather small.

2.5 Potentials

For the atomic screened Coulomb potential, Lindhard used the so-called standard potential, an analytical, easy-to-evaluate potential,

$$V(r) = \frac{Z_1 Z_2 e^2}{r}\left(1 - \frac{r}{(r^2 + C^2 a^2)^{1/2}}\right) \tag{10}$$

which leads to the critical angles ψ_1 and ψ_p, Eq. (6).

The corresponding single-string axial continuum potential is obtained from Eq. (1)

$$U(r_\perp) = \frac{Z_1 Z_2 e^2}{d} \ln\left(1 + \frac{C^2 a^2}{r_\perp^2 + \tfrac{1}{2}\rho^2}\right) \tag{11}$$

where d is the distance between the atoms in the string, and where the thermal averaging, Eq. (8), has been approximated introducing the $\frac{1}{2}\rho^2$ term.

The corresponding planar continuum potential, for a single static plane, is obtained from Eq. (2),

$$U(y)=2\pi Z_1 Z_2 e^2 N d_p[(y^2+C^2a^2)^{1/2}-y] \tag{12}$$

where y is the distance from the plane and d_p is the planar distance.

A rather accurate potential, for more quantitative evaluations, is the thermally averaged Doyle-Turner single-string potential given by

$$U(r_\perp) = \frac{Z_1 e^2}{a_0}\frac{2a_0^2}{d}\sum_{i=1}^{4}\frac{a_i}{B_i+\rho^2}\exp(-\frac{r_\perp^2}{B_i+\rho^2}) \tag{13}$$

where $B_i = b_i/4\pi^2$, and the constants a_i and b_i are given in Table 1 for silicon and germanium. The corresponding planar thermally averaged Doyle-Turner potential takes the form

$$Y(y)=2\sqrt{\pi}Z_1\frac{e^2}{a_0}a_0^2 N d_p\sum_{i=1}^{4}\frac{a_i}{(B_i+\rho^2)^{1/2}}\exp(-\frac{y^2}{B_i+\rho^2}) \tag{14}$$

Axially channeled particles are moving in a potential which is the superposition of the single-string potentials pertaining to the individual strings in the transverse plane, see Fig. 2 b). There is, however, only a significant difference between the multi-string and the single-string potential for small transverse energies. Similarly, the planar potential is the sum of the two potentials from neighbouring planes.

Table 1
Parameters for Doyle-Turner potential

Si		Ge	
a_i [Å]	b_i [Å^2]	a_i [Å]	b_i [Å^2]
2.1293	57.7748	2.4467	55.893
2.5333	16.4756	2.7015	14.393
0.8349	2.8796	1.6157	2.4461
0.3216	0.3860	0.6009	0.3415

2.6 Dechanneling

The thermal vibrations of the crystal atoms, the discreteness of the lattice and the presence of the electrons in the target mean that the motion in the continuum potential is perturbed, and changes in the transverse energy take place. On the average the transverse energy will increase with penetration depth. This means in particular that channeled particles may become transferred to the random beam, a process called *dechanneling*. For low transverse energies, it is the scattering on the electrons which contributes, whereas for higher

transverse energies it is the nuclear scattering which dominates. In general the dechanneling process can be described by a diffusion equation. For well-channeled particles, in particular planar channeled, the dechanneling process can be approximated by an exponential depletion of the number of channeled particles,

$$n = n_0 \exp(-z/L_0) \tag{15}$$

where the phenomenological dechanneling length L_0 scales with momentum. For the (110) plane in silicon, $L_0 \approx 0.9\text{m}\cdot p[\text{TeV/c}]$. The inverse process of dechanneling is also possible and random particles may become channeled. This process is called 'feed-in' or 'volume capture'.

For not too small transverse energies, the dechanneling is dominated by scattering on the nuclei. This means that there is a temperature dependence of the dechanneling length owing to the thermal vibrations, and channeling effects can be enhanced by cooling the crystal.

In Fig. 4 are shown some measurements of proton dechanneling lengths at high energy for the (110) plane in silicon at room temperature demonstrating the energy scaling.

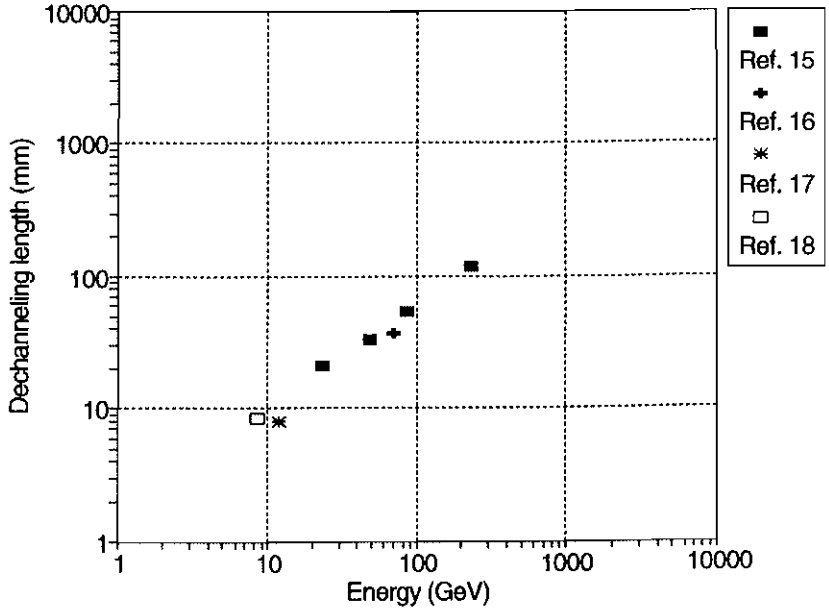

Fig. 4 Measurements of dechanneling lengths in silicon

The dechanneling lengths for negative particles are much shorter than for positive, because negative particles move in areas of high electron and nuclear density.

2.7 Crystals and Radiation Damage

To observe channeling effects and to apply them, it is clearly neccessary to have single crystals, or polycrystalline material with a mosaic spread much less than the relevant critical angles. At high energy, this leaves only silicon, germanium and more recently diamond as target materials. These materials all have diamond structure. At low energy many other crystals are available for channeling.

It is also important that the crystals are almost perfect in other respects, namely the number of defects should be small. There exists many types of defects in crystals, originating either from displaced crystal atoms, dislocations, or impurities. It is obvious that atoms sitting

in the channels between the strings or planes lead to increased dechanneling. Actually, low-energy channeling can be used to identify the lattice positions of impurities. Hence it is important, that the crystal material has a small number of impurities and defects. Radiation damage, that is damage of the crystal owing to the beam exposure, will also lead to an enhanced dechanneling. A close collision between the projectile and a lattice atom may displace the lattice atom from the string position to an interstitial position, and create a vacancy. In general, such point defects are less severe at high energy, where the cross section for scattering to large angles is small and where the number of atoms participating in one collision with a string is enormous ($\sim 1/\psi_1$).

3. THE STRONG FIELD AND ITS ORIGIN

It is well-known from Coulomb's law

$$E(r) = \frac{Z_2 e}{r^2} \tag{16}$$

that very high electric fields exist close to point-like particles. For example, the electric field at a distance of 0.1 Å from a silicon nucleus amounts to $2 \cdot 10^{12}$ V/cm. This high field is, however, not of much use as a deflecting field, since it only extends over distances ~0.1 Å.

In the continuum approximation, we have for a <110> string of silicon atoms $E \sim 1.3 \cdot 10^{10}$ V/cm corresponding to a magnetic field (for relativistic particles) of 4000 Tesla. Furthermore, this field extends all along the length of the string, i.e. over the macroscopic distance of the crystal thickness (from mm to m). In the planar case, the corresponding field is $1.3 \cdot 10^9$ V/cm (~ 400 Tesla), and this field applies all over the extent of the two-dimensional plane. It is these immense fields extending over macroscopic distances, which makes channeling useful for the deflection of charged particles.

For crystals of higher atomic number than silicon, the fields are evidently larger than the values given above.

4. MANIFESTATIONS OF CHANNELING

Channeled positive particles are kept away from the strings and planes of atoms, whereas negative particles are focused around the atomic strings and planes. This will obviously change the interaction between the projectiles and the crystal atoms. In the following, examples of such channeling effects will be presented, and again the emphasis will be on qualitative features.

4.1 Scattering of Channeled Particles

Let us first consider the scattering phenomena occurring when particles are channeled through a crystal. Multiple scattering of transmitted particles is mainly due to scatterings on the nuclei, screened by the electrons, and to a lesser extent to scattering on the electrons. Hence well-channeled positive particles will have a reduced multiple scattering, whereas the multiple scattering of negative particles will be increased. This effect is clearly demonstrated in so-called transmission experiments, where the intensity in incident-angle space of particles scattered less than some finite angle is observed. In particular for crystals, where the random multiple scattering angle is larger than the critical channeling angles, the crystalline structure emerges clearly. For example, in Fig. 5 (left), this distribution is shown for 10 GeV protons transmitted through a 0.3 mm thick <110> Ge crystal [19,20]. The maximal scattering angle

is 0.1 mrad, ψ_1 = 0.22 mrad and the rms multiple scattering angle θ = 0.16 mrad. The high transmission along the axial and planar directions is evident, and even weak (high-index) planes are seen. For negative particles the opposite effect is expected, but since the increased multiple scattering also leads to a strong dechanneling, the effect is not as easily visible [20].

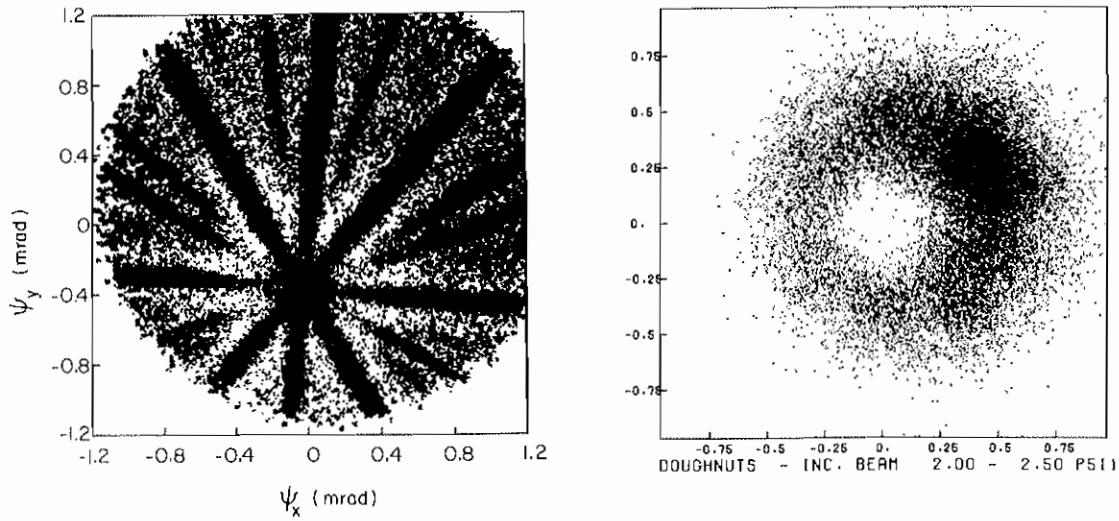

Fig. 5 Left: Incident angle distribution of 10-GeV protons transmitted through a 0.3 mm <110> Ge crystal with small scattering angles; Right: Exit-angle distribution, "donut", of 10-GeV protons transmitted through a 0.6-mm <110> Ge crystal. The particles are incident at an angle of 2-2.5 ψ_1.

Another scattering phenomenon for axially channeled particles, namely "donut" scattering, is observable for both positive and negative particles [20]. This effect originates from the conservation, at least approximative, of transverse energy, which means that the polar angle to the axis is conserved. This means that a narrow beam incident close to an axial direction will produce a donut shaped distribution at the exit side of the crystal. In particular at high energy, where the transverse energy is approximately conserved far outside the critical channeling angle, such donuts can be seen. For example, in Fig. 5 (right) is shown the exit-angle distribution of 10 GeV protons transmitted through a 0.6 mm <110> Ge crystal [20]. The beam is incident at polar angles of 2-2.5 ψ_1, and with an azimuthal angle corresponding to "2 o'clock". The azimuthal scattering is seen with a maximum at the incident direction, and with some radial smearing corresponding to transverse energy changes.

4.2 Close-encounter Processes

Close-encounter processes, which require a small-impact parameter collision with a target atom, will have a decreased/increased probability for aligned positive/negative particles. An example of such a process is wide-angle scattering. In Fig. 6 is shown the normalized (to random incidence) yield of wide-angle scattering as function of incident angle to the <110> axis for 15 GeV protons traversing a 4.2 mm Ge crystal [20]. A reduction in the wide-angle scattering yield of more than an order of magnitude is seen. The curve is a calculation taking dechanneling and angular resolution into account. Only fair agreement is obtained. This is partly owing to experimental problems, since scattering angles of more than 17 ψ_1 are very improbable leading to a poor signal to background ratio. This very large minimal scattering angle was chosen in order to exclude effects from donut scattering. The characteristic angle for such dips is seen to be the critical channeling angle ψ_1.

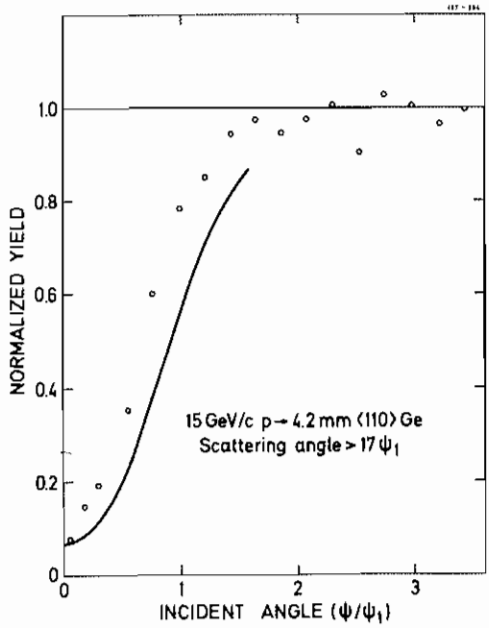

Fig. 6 Normalized wide-angle scattering yield as function of incident angle

4.3 Electronic Processes

The channeling effect also shows up in the interaction with the atomic electrons. In particular for the excitations of inner-shell electrons are channeling effects present. Although the excitations may be both close and distant for particles with $\gamma >> 1$, reductions in inner-shell excitation yields are seen for both axial and planar channeled positive particles [21]. Actually by using particles of increasing γ the influence of distant collisions may be revealed [21]. For negative particles an increased yield relative to random incidence is observed [21].

Another electronic process, which has been investigated is emission of δ-rays, i.e. hard knock-on electrons [19]. Such electrons can only be produced in close collisions, and hence the δ-ray yield is proportional to the electron density along the projectile trajectory. Since channeling allows control of the trajectories in the transverse plane, such measurements reveal information about electron densities. In Fig. 7 is shown the δ-ray yield as function of incident angle to the <110> axis for 11.9 GeV protons incident on a 0.54 mm Ge crystal [19]. The measurements are compared to calculations for two different electron density-models, and good agreement is seen. Reductions (up to a factor of two) are also seen in the δ-ray yield for planar channeled positive particles, and negative channeled particles do give an increased yield [19].

A process of both practical and fundamental relevance is the electronic energy loss, that is the energy loss of particles stemming from excitation of the electrons. This energy loss involves both close and distant collisions. In Figs. 8 and 9 are shown the energy-loss distributions for both random and axially (<110>) and planar ({110}) channeled particles passing a 0.74 mm Ge crystal [22]. For random incidence the energy-loss distribution is the so-called Landau distribution. For the axially aligned particles a reduction by almost a factor of two is seen in the most probable energy loss, and for planar channeled particles smaller reductions are observed, in particular for the weaker planes.

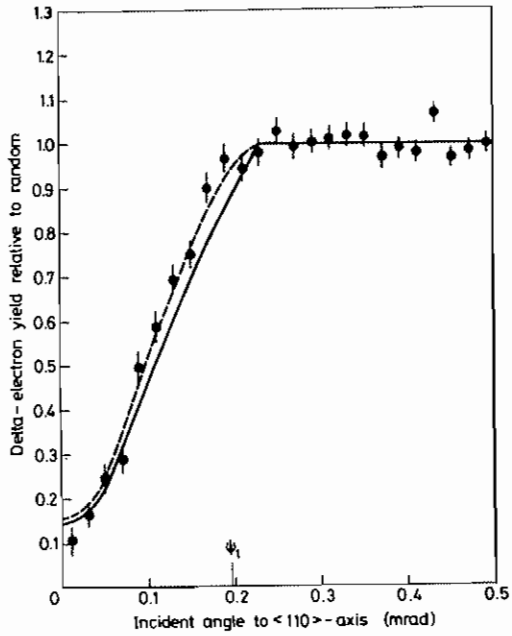

Fig. 7 Measured and calculated δ-ray yield as function of incident angle

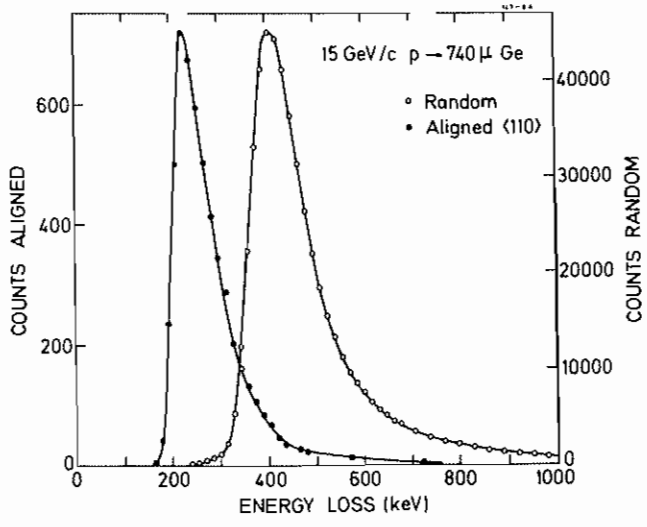

Fig. 8 Energy-loss spectra in Ge for axially channeled and random positive particles

For negative particles an increased energy loss is seen, although the dechanneling is diminishing the effect. In Fig. 10 is shown the energy-loss distribution of 15 GeV negative pions traversing a 0.74 mm Ge crystal along the <110> axial direction [22]. As can be seen, channeling mainly influences the tail of the distribution, produced by close collisions with the atomic electrons, i.e. a local process.

4.4 Channeling Radiation

Electrons and positrons traversing material radiate photons, bremsstrahlung. The spectrum of the radiated photons is the so-called Bethe-Heitler spectrum, characterized by an inverse energy dependence of the radiation probability. The probability is characterized by the so-called radiation length, which in silicon and germanium is 9.36 and 2.30 cm, respectively.

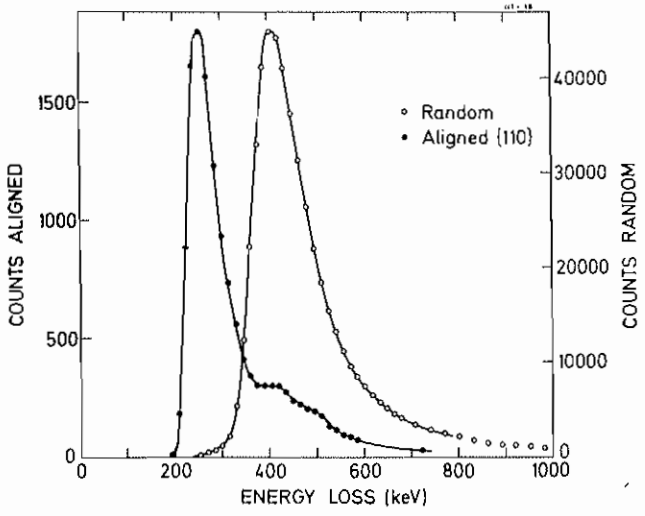

Fig. 9 Energy-loss spectra in Ge for planar channeled and random positive particles

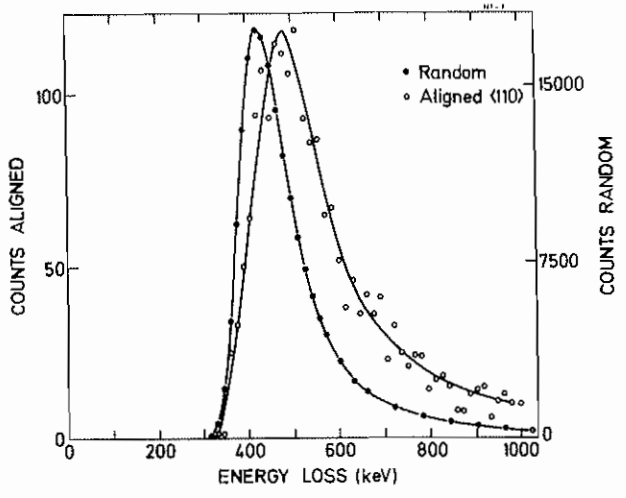

Fig. 10 Energy loss spectrum in Ge for axially channeled and random negative particles

Channeled electrons/positrons have an increased emission of bremsstrahlung. The regular motion of electrons/positrons through single crystals lead to coherent emission of high-energy photons, in much the same way as undulators used in electron storage rings force the electrons to wiggle up and down and radiate photons. This channeling radiation can also be viewed as transitions between bound states in the transverse potential. In Fig. 11 are shown channeling radiation spectra for 6.7 GeV positrons and electrons traversing a 0.105 mm Si

crystal along the {110} planes [23]. For electrons and positrons in the 10-GeV range the photon energies are in the tens-of-MeV range. We see enhancements, relative to random incidence, of up to a factor of 50. For positrons, the planar potential is almost harmonic, leading to a spectrum consisting of peaks corresponding to the first and higher harmonics of the fundamental energy. For electrons the potential is anharmonic leading to a featureless photon spectrum. The measurements are compared to calculations based on classical electrodynamics, and good agreement is obtained.

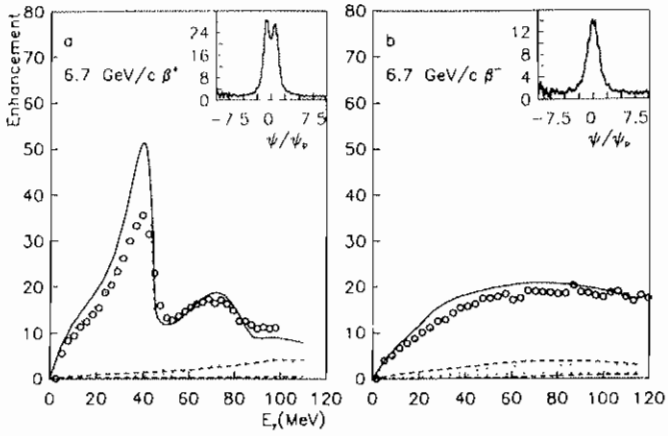

Fig. 11 Channeling radiation spectra for planar-channeled 6.7-GeV positrons and electrons

For much higher energies, the energy of the emitted photons may be a significant fraction of the primary energy, and quantum electrodynamics is required to describe the process. The situation is here in the same regime as beamstrahlung in electron/positron colliders, the process of photon emission from electrons in the electric field of the positron bunch or vice-versa. As an example we present in Fig. 12 the photon spectrum for 150 GeV electrons traversing a 0.4 mm Ge crystal at various angles to the <110> axis [24]. We observe large enhancements up to a factor of 60 and furthermore that the spectrum extends all the way to the energy of the incident electron. The peak is explained as a multi-photon peak, and each electron radiates tens of photons. Note also, that the well-aligned eletrons radiate on the average half of their energy in 0.4 mm Ge! For production of single high-energy photons, there are incident angles close to the axis, where these photons are emitted with high probablility [25]. Let us mention, that positrons also radiate with enhanced probability relative to random, although not as intensely as electrons for well-aligned projectiles.

Channeling radiation is intimately connected to coherent bremsstrahlung emitted when electrons or positrons cross crystalline planes or strings of atoms.

Finally, we note that channeling radiation photons are polarized.

4.5 Pair Creation

The inverse process to this channeling radiation, namely pair production by photons, is also increased in aligned crystals. In Fig. 13 is shown the measured pair production yield as function of photon energy for photons incident within 0.25 mrad of the <110> axis in Ge compared to a calculation [26]. Above an energy threshold, 25 GeV for Ge <110>, the enhancement increases almost linearly. This threshold is lower in energy the deeper the axial potential. Hence it is especially low for strong axes in high-Z materials. Crystals may obviously be usefull as bremsstrahlung and pair-production targets.

The combination of an increased bremsstrahlung and pair-production yield leads to an increased shower formation in single crystals [27]. In other words, a shower initiated by a photon or electron/positron develops over much shorter distances in an aligned crystal.

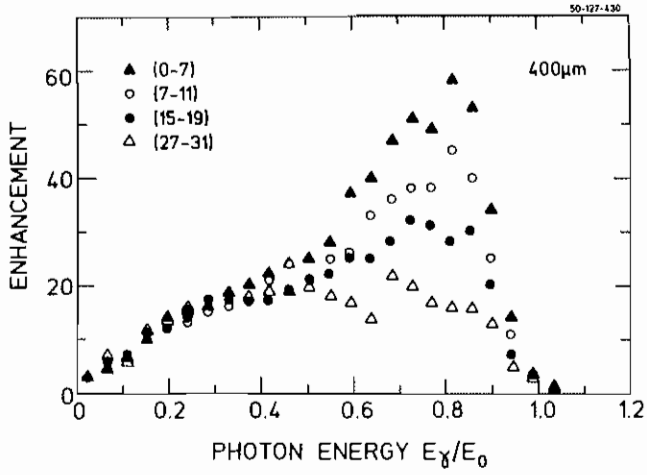

Fig. 12 Enhancements of photons for 150-GeV electrons incident on a 0.4-mm Ge crystal

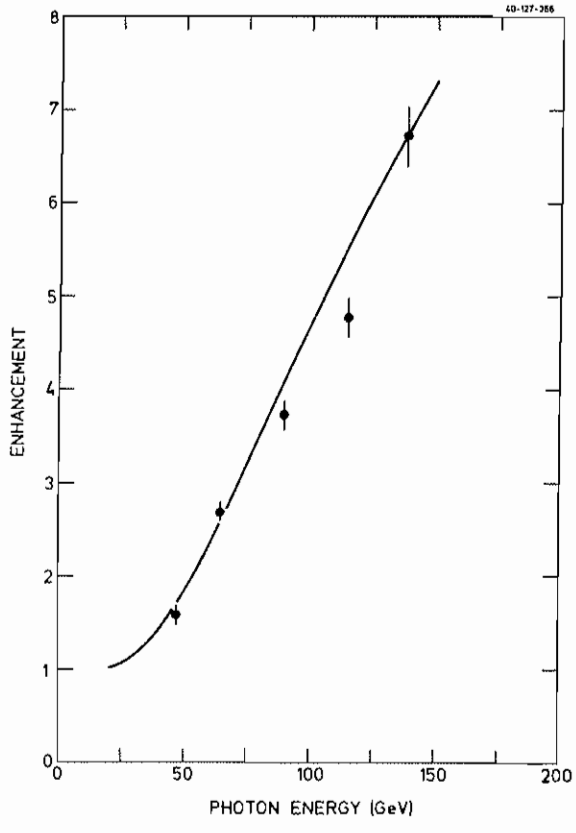

Fig. 13 Pair production yield for photons axially aligned photons in a Ge crystal.

4.6 The Universality of the Channeling Description

The channeling model, and these channeling effects, have been studied for a number of different projectiles: electrons/positrons, muons, pions, protons and heavy ions. The energies

used range from keV to TeV corresponding to critical angles from degrees to microradians, and the same, relatively simple, description of particles colliding with strings or planes of atoms holds over this enormous energy range. Note, that at high energy ($v \approx c$), the channeling properties of a particle only depend on its charge and momentum.

The study of channeling and the applications of the effect have yielded a wealth of results in both applied and basic research. In particular at low energies, standard techniques using channeling are today widely used in e.g. semiconductor and materials science. At high energy, the application of the channeling effect is less mature, but several developments have started as we are going to see now.

The reader is referred to the bibliography for further details and references to the large subject of channeling effects.

5. CHANNELING IN A BENT CRYSTAL

In the following we shall confine ourselves to planar channeling of positive particles.

It is hardly surprising, that also when a crystal is slightly bent elastically, planar channeled particles will still follow the bent planes. Channeling in a bent crystal with constant curvature is described in the continuum approximation by the introduction of a centrifugal force, giving rise to an effective potential

$$Y_{eff}(x) = Y(x) - \kappa pvx \tag{17}$$

where x is the distance from the centerline between the atomic planes. The curvature is given by $\kappa = 1/R$, where R is the radius of curvature. In Fig. 14 is shown the potential from an unbent crystal (full-drawn curve) and the resulting potential for a bent crystal, in the case of $R = 4$ m (dotted) and $R = 15$ m (dash-dotted) at $pv = 450$ GeV. It is seen, that bending will cause particle trajectories to shift towards the outer atomic plane, and that bending leads to a lowering of the potential barrier. In this way, the critical angle of a bent crystal is reduced.

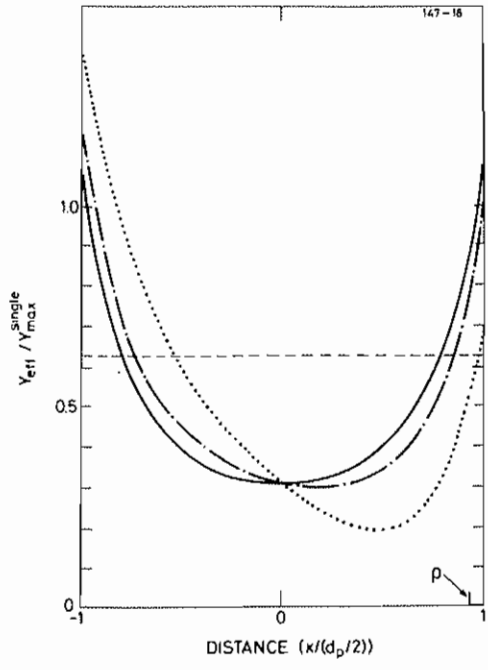

Fig. 14 Planar potential for a straight (full-drawn curve) and bent crystals

As was realized by Tsyganov [11], there is a critical radius of curvature R_c for which there is no potential well, i.e. no channeling. This critical radius is reached when Y_{eff} has a minimum at $x = d_p/2$ (or rather $d_p/2$ - ρ), which gives

$$R_c = pv/\pi Z_1 Z_2 e^2 N d_p. \tag{18}$$

Only at high energies can crystals be bent elastically to this limit. For (110) planes in Si we get $R_c = 0.4\text{m}\cdot p[\text{TeV/c}]$. This is a very large curvature, corresponding to 4.3 degrees or 75 mrad over 3 cm at 450 GeV!

It is practically not possible to bend a crystal all the way to the edge, and hence there is always a straight entrance, and exit, part of the crystal. This straight part is a useful position for a semiconductor detector which, as we will see later can be used to 'tag' channeled particles.

The influence of the bending is usually described by a bending dechanneling function, the fraction of charged particles lost from the channeling regime (with transverse energies $E_\perp \rangle Y_{eff}(d_p/2 - \rho)$) [28,29]. This dechanneling fraction F is given in Fig. 15 from Ref. [15]. It is only accurate for a uniformly populated transverse phase space, i.e. for a beam divergence larger than ψ_p. The abscissa coordinate is a normalized curvature and momentum variable, $\Gamma = \frac{1}{2}\kappa R_c = \frac{1}{2}R_c/R$. Furthermore the bending leads to a modification of the multiple scattering dechanneling, since the average position of the particles shifts towards the atomic planes with higher electron and nuclear densities. It can be approximated by $L_B = L_o(1-F)^2$.

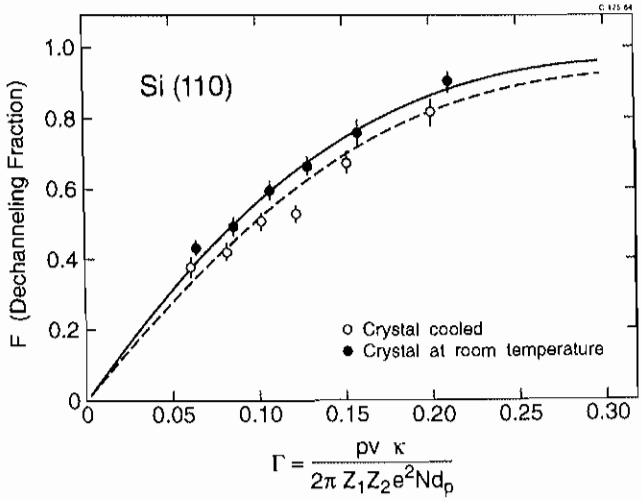

Fig. 15 Dechanneling fraction as function of normalized curvature

An accurate prediction of the bending efficiency requires a detailed simulation. A rough estimate can be made from the following prescription: 1) The surface transmission, i.e. the number of initially channeled particles, is calculated from e.g. Fig. 3 for a given beam divergence. 2) The multiple scattering dechanneling is taken into account by application of the depletion, Eq. (15). 3) The bending dechanneling is calculated from Fig. 15. The influence of the bending on the normal dechanneling is introduced. It should be noted, that this procedure is only valid for a uniform curvature. For a non-uniform curvature, the most important modification is to determine the bending dechanneling from the maximum curvature in the crystal, which as we will see later can be significantly larger than the average curvature.

6. BENDING BEAMS WITH CRYSTALS

The first observation of beam bending was made at JINR, Dubna at 8 GeV in 1978 [12], two years after the proposal. Since then, bending has been performed up to energies of 800 GeV [30]. Axial bending [17] is much less studied than planar. Planar bending of negative particles has never been investigated experimentally. All the experiments [12,13,15-18,30-38] have been made with protons, apart from [17] and [31] where π^- and C^{6+}, respectively, were used. These previous bending experiments are summarized in Table 2. We shall in the present paper concentrate on the recent CERN experiments, first of all because the author has been involved in these experiments, but also because only in these recent 450 GeV experiments, large efficiencies up to 50 % have been obtained. Before discussing this experiment in detail, let us look at the, at first sight trivial, problem of bending a crystal.

Table 2
Bending experiments

Year	Energy	Laboratory	Bending details	Ref.
1979	8.4 GeV	JINR, Dubna	2 cm, 1-26 mrad	12
1980	12 GeV	CERN	3 cm, 4-52 mrad (p,π^+,π^-)	13, 17
1982	1 GeV	Leningrad	0.1-1 cm, (also focusing)	33, 38
1984	12-800 GeV	Fermilab	2-5 cm, 3-32 mrad	15, 30, 32
1987	53 GeV/c	JINR, Dubna	2 cm, 65 mrad, (C^{6+})	31
1989	450 GeV	CERN (H8)	5 cm, 2-12 mrad	34, 35
1989	450 GeV	CERN (H4)	5 cm, 10 mrad	36
1991	70 GeV	IHEP, Protvino	7-10 cm,20 mrad, focusing	16, 37

6.1 Bending Devices

The ideal beam bender is a crystal bent at constant curvature, so that the crystalline planes make a section of concentric cylinders. In practice some mechanism is needed to bend the crystal as closely as possible to this ideal curvature.

Historically, the first bending devices used were three-point benders as in Fig. 16 a), where three parallel rods are pressed onto the flat sides of the crystal, to bend it. Ideally, such a bender gives a linearly increasing curvature from the first rod to the middle and a correspondingly decreasing curvature from the middle to the last rod. In this way, the maximum curvature is twice the average curvature.

The obvious improvement to the three point bender is a four-point bender, as in Fig. 16 b), where ideally the curvature is linearly increasing from the first rod to the second, then constant from the second to the third and then finally linearly decreasing from the third to the fourth rod. A common problem to the three and four point bender is the local distortions at the contact points of the rods, which lead to additional dechanneling, in particular at the points of the crystal side in direct contact with the rod. This local stress is observable experimentally as additional dechanneling at the deflection angles corresponding to these points (see later).

An elegant way to avoid mechanical stress and produce a uniform bend is to bend the

crystal by coating one side of the crystal with a layer of a different material. In Ref. [15] a 26 mm Si crystal was bent 30 mrad by sputter coating one side of the crystal with a 10 micron layer of ZnO. Obviously, the resulting bending angle is not adjustable, and it is temperature dependent. Furthermore, the coating also produces a transverse bend.

Approximately uniform bends have also been obtained by pressing crystals against precision machined cylindrical surfaces. The crystals have been pressed either by rods at the crystal ends [36] or by a 'fluid' composed of small steel balls [34]. Also in this case, the bending angle is fixed. However, the beam bending angle can be adjusted by using the long sides of the bent crystal as entrance and exit faces [36].

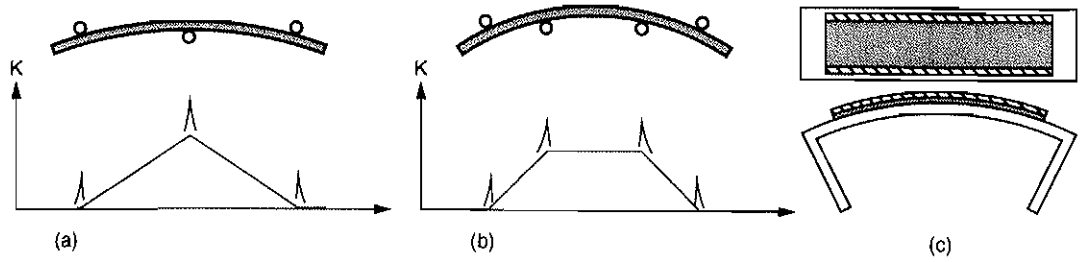

Fig. 16 Crystal benders of 3-point, 4-point and U-type. The graphs show the curvature along the crystals for the 3- and 4-point benders.

Finally, the bottom of a U-shaped piece is bent uniformly by pressing the top of the two sides together, Fig. 16 c). So if a crystal is clamped to such a U-shaped stainless steel piece, the crystal will be approximately bent cylindrically. Even better, the crystal itself can be machined to the shape of a U. In this case, bending in the unwanted directions, in particular variation of the planar direction with position on the entrance side of the crystal, can be avoided. Such crystals have been used in the CERN extraction experiments to be discussed in Section 7.

6.2 The 450-GeV CERN Bending Experiment

The recent 450-GeV experiments at CERN have been made in two beamlines in the north area of the SPS. At the H4 beam, experiments have been performed as a preparation to the use of a crystal in the new CP-violation experiment NA48 [36,39]. The other experiments [34,35], which we will discuss in some detail, are made in the H8 microbeam, which is a unique beam for such investigations. This beam has an extremely small emittance, obtained by successive collimation of the primary beam. At the position of the crystal, the beam size is around 2×1 mm^2 (FWHM) to be compared to the crystal size of 0.9×10×50 mm^3. Furthermore, the horizontal divergence is around 3 μrad (rms) to be compared to ψ_p = 7μrad for (110) Si at 450 GeV. The beam intensity is up to a few 10^6 protons per burst.

Different bending devices have been used in these experiments, but we shall confine ourselves to the discussion of the results obtained with a 3-point bender. The layout of the experiment and the bending jig are shown in Fig. 17 a) and b), respectively. The bent silicon crystal is mounted on a goniometer with 1.7 μrad stepsize. Scintillators (SC) 1, 2 and 3 are used to define a beam trigger, with scintillator 4 as a veto of events creating a nuclear interaction in the crystal. Two drift chambers (DC) are used to measure the position of the beam particles just in front of the crystal and 4 meters behind. Data were accumulated with bending angles from 1 to 11 mrad.

A surface-barrier semiconductor detector is produced on the straight entrance part of

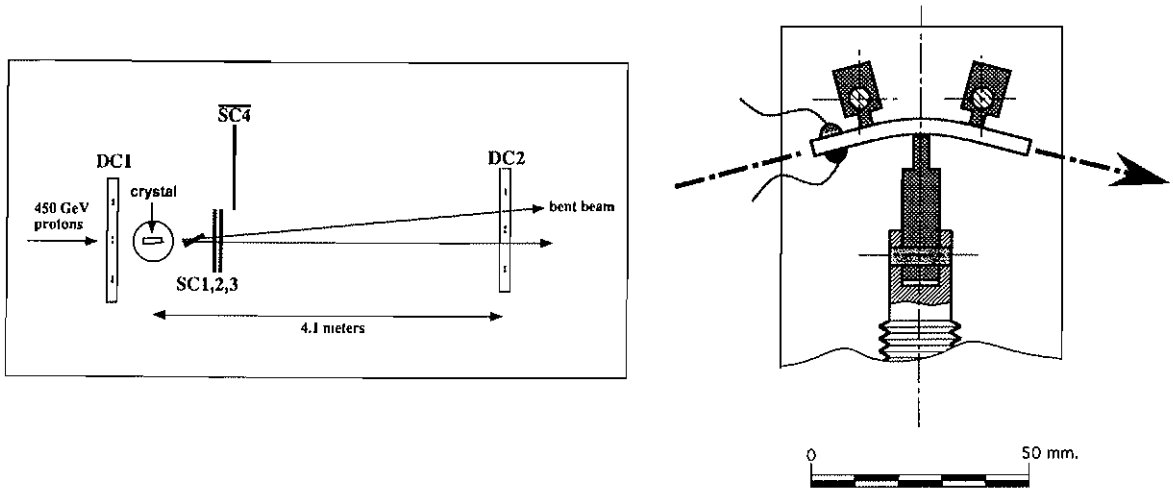

Fig. 17 a) Layout of bending experiment. b) Crystal bender.

the crystal to tag the channeled particles (Fig. 17 b). In Fig. 18 a) and b) are shown the energy-loss spectra for a non-aligned beam and for a beam aligned with the (111) planes of the silicon crystal. The usual Landau distribution is seen in Fig. 18 a) (with some background) and for an aligned beam in Fig. 18 b) we observe the low-energy loss channeled particles. From Fig. 18 b) we deduce immediately a channeled fraction of the beam upon entrance in excess of 50 %. In Fig. 18 b) is also plotted the energy loss of those particles deflected 8.9 mrad by the crystal. A narrow energy-loss distribution is observed without a random component, meaning that the bent particles are all channeled from the entrance of the crystal, i.e. no feed-in (Section 2.6).

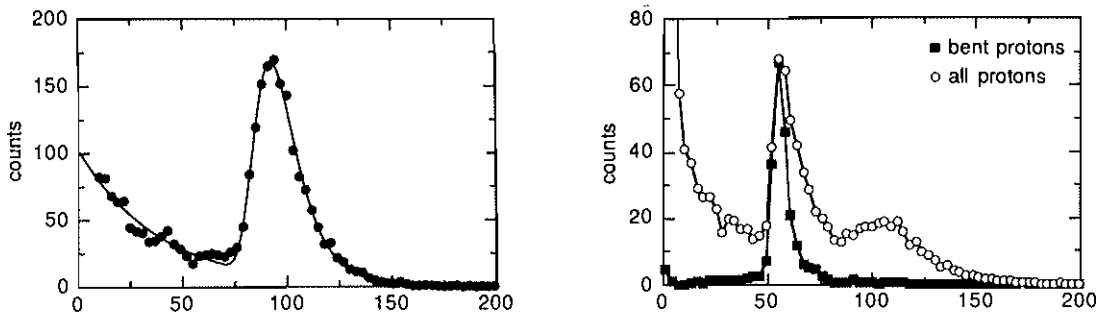

Fig. 18 Energy-loss distributions for a) random and b) aligned crystal

The crystal acceptance can be measured by monitoring the channeled particles, either by their low-energy loss or by bending, as a function of crystal angle. In Fig. 19 a) is shown the energy-loss window used to tag the channeled particles, and in Fig. 19 b) the measured crystal acceptance. The steepness of the distribution demonstrates that the beam indeed has a very small divergence. The FWHM of the distribution is 17 μrad to be compared to twice the critical angle, i. e. 14 μrad.

The distributions of the deflected and straight beam, as measured by the second drift chamber are shown in Fig. 20, for crystal bendings of 2.4, 4.6 and 8.1 mrad. The left-most peak is the undeflected beam, and the right-most peak is the bent beam. Between these peaks are the dechanneled particles. The tail from the unbent beam to the middle is the particles

dechanneled because of the increasing curvature, whereas from the middle to the bent beam there are very few particles, namely only those dechanneled because of multiple scattering. We also observe, in particular for the 4.6 mrad bending angle, the excess dechanneling caused by the local stress at the middle pin.

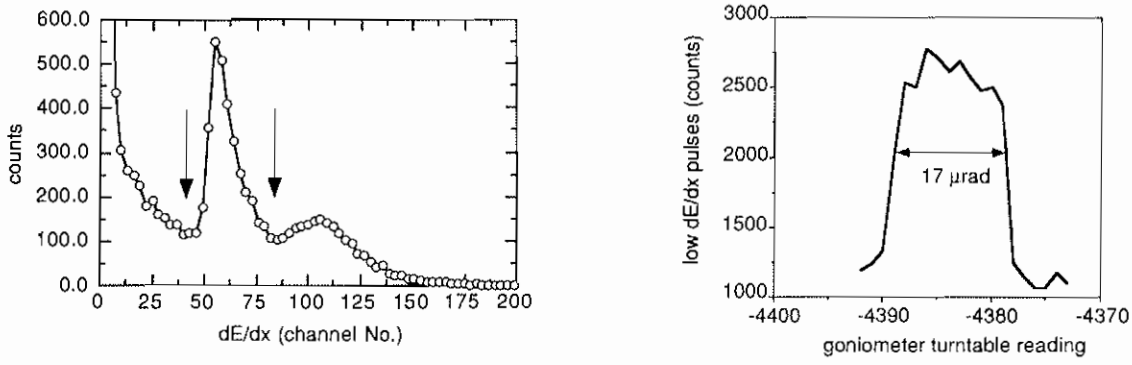

Fig. 19 a) Low-energy loss window. b) Crystal acceptance.

The efficiency can be deduced by measuring the number of bent particles relative to the number of incident particles from data as in Fig. 20. This has been done for nine different bending angles, and the resulting efficiencies as function of bending angle are shown on Fig. 21. The efficiency varies from almost 50 % at 1.4 mrad to 1 % at 11 mrad. The measurements are compared to calculated efficiencies using two extreme models for the curvature. The actual curvature of the crystal bent in the three-point bender is not known, but it is expected to be in between the ideal three-point bender and a uniform-curvature bender. Remember here, that it is the maximum curvature that determines the bending dechanneling. There is a fair agreement between the measurements and the calculations, as the measurements fall in between the two extremes.

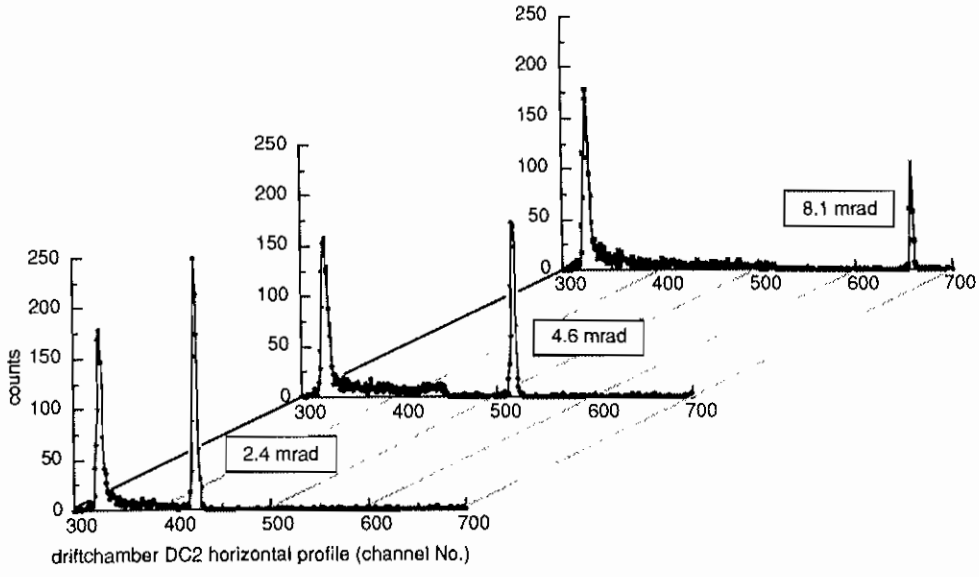

Fig. 20 Profiles of the deflected beams 4 meters downstream of the crystal

Let us here also mention, that channeling in bent crystals allows measurement of

magnetic moments of elementary particles as has been demonstrated for Σ^+ in [40].

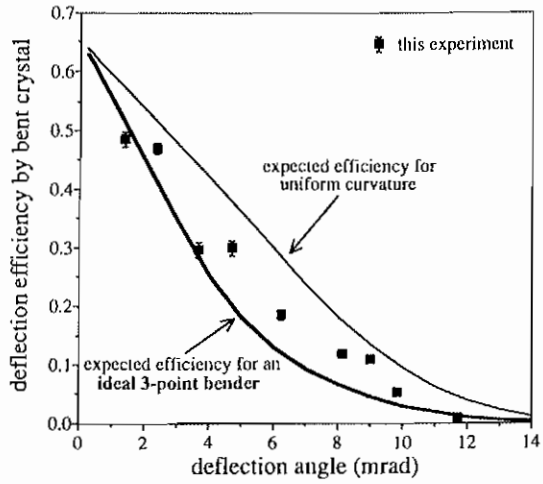

Fig. 21 Measured and calculated deflection efficiencies

6.3 Focusing With Crystals

Bent crystals can also be used for focusing beams. Focusing can be performed in different ways, e.g. by shaping the exit face of the bent crystal [37] or by using a crystal bent perpendicular to the beam direction [38]. Very short focal lengths (~ meter) and very small beam sizes can be obtained, even at high energies.

7. EXTRACTING BEAMS WITH CRYSTALS

Since a crystal can, to some extent, replace a magnet in a beam line, it can also be used as a septum magnet in a synchrotron/storage ring. The advantage of using a crystal to replace a conventional septum magnet is not only the large deflection power, but maybe more the inherently small septum thickness. The effective septum thickness of a crystal septum is ideally extremely small, namely the planar distance. In practice it will be appreciably larger, determined by surface roughness and miscuts.

Several extraction experiments have already been made, and some details are given in Table 3. Again, we shall mainly confine ourselves to the CERN experiment for the reasons given above.

Table 3
Extraction experiments

Year	Energy	Laboratory	Crystal length, Bending angle, Efficiency	Ref.
1983	4.2-7.5 GeV	JINR, Dubna	1.1 cm, 35 mrad, ~ 10^{-4}	41
1990-	50-70 GeV	IHEP, Protvino	7 cm, 80 mrad, < 0.7 %	42
1992-	120 GeV	SPS, CERN (LHC)	3 cm, 8.5 mrad, 10 %	43
1994-	900 GeV	Tevatron, Fermilab	1.1 cm, 0.6 mrad	44

The attractive feature of using a crystal to extract a beam from a circular accelerator is, besides the inherently small septum thickness, the fact that it works just as well, and in some respects better, the higher the beam energy owing to the decreasing dechanneling length with energy.

Extraction channels in accelerators typically consist of a system of electrostatic and magnetic septum magnets. The first element is usually an electrostatic septum consisting of a long array of thin wires. As an example, we take the CERN SPS [45], where the electrostatic septum consists of three 5 m long arrays of < 0.1 mm thick wires used to produce a field of 120 kV/cm. This septum gives a deflection of 0.4 mrad at 450 GeV. Obviously, for the 7 TeV LHC beam, the length of a conventional wire septum would be enormous, and there would be severe alignment problems. On the other hand, a bending angle of a fraction of a mrad for a silicon crystal for the same 7 TeV beam can easily be envisaged.

A crystal can be used as a septum magnet in at least two different ways. In Fig. 22 are shown schematically two scenarios of 'scraping' the beam with two different edges of the crystal. In both cases, the effective septum thickness will be given by the surface roughness, i.e. it is important that the surfaces are polished (without damage) to optical quality. Furthermore it is essential in (a), that the angle between the extracting surface and the planar direction is very small.

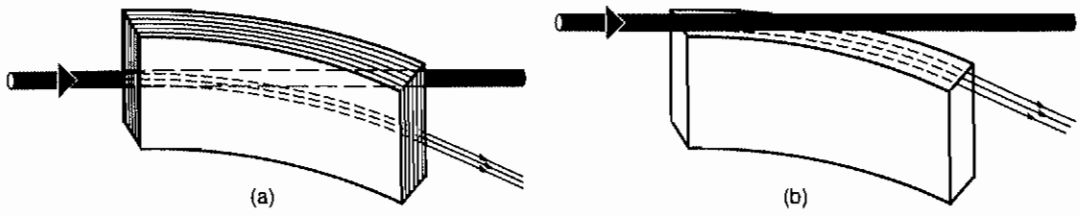

Fig. 22 Scenarios for crystal extraction

The lay-out of crystal extraction is shown in more detail in Fig. 23. Here the importance of surface roughness and miscut angle is evident. It is furthermore seen, that the impact parameters of the particles incident on the crystal should be large compared to the surface roughness, and that the impact angles should be less than the critical angles.

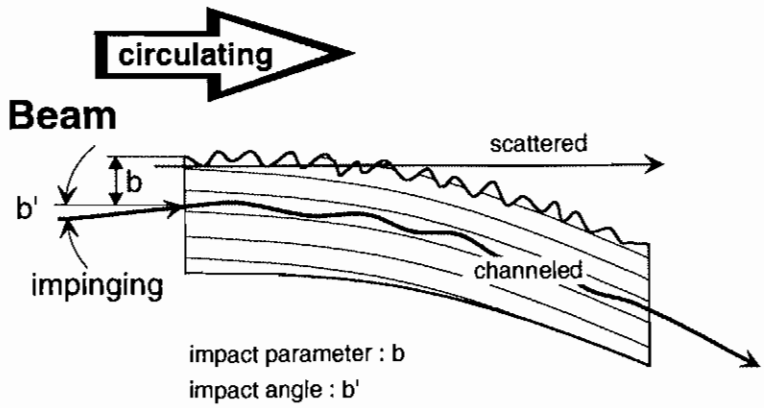

Fig. 23 Impact of beam particles on crystal

The extraction efficiency can be calculated as outlined in Section 5. Calculated efficiencies are shown in Fig. 24 as function of pv/R for four bending angles. For a given bending angle, there is a maximum in the efficiency, since the bending dechanneling is increasing for decreasing R, and the multiple-scattering dechanneling increasing for increasing R, i.e. longer crystals. The maximum efficiency for an extraction angle of 8 mrad is 42 % for pv/R = 0.4. This gives for the SPS-energy of 120 GeV an optimal crystal length of 2.4 cm. For an extraction angle of 0.2 mrad (relevant for the LHC), the maximum efficiency is 74 % at pv/R = 0.07, corresponding to a crystal length of 20 cm at 7 TeV.

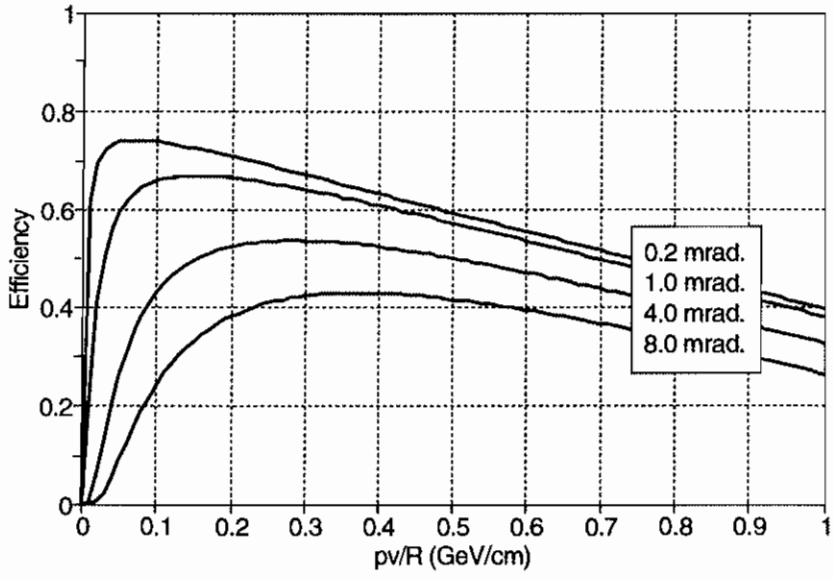

Fig. 24 Calculated bending/extraction efficiencies for Si (110)

7.1 The CERN Extraction Experiment

The motivation for the extraction experiment at the CERN SPS was the possibility to extract parasitically a proton beam from the LHC for fixed target physics (CP-violation in the b-quark system) [46]. The Large Hadron Collider is a planned superconducting 7+7TeV collider to be built in the LEP tunnel at CERN. An extracted beam of intensity 10^8/sec. would provide 10^{10} BB-bar pairs per year, two orders of magnitude more than from an e^+e^- B-factory with the very large luminosity $\mathcal{L}=10^{34}cm^{-2}s^{-1}$. At the nominal luminosity in the LHC, around 10^9 protons per second are expected to diffuse from the central core of the LHC beam (10^{14} protons) into the halo, where they will have to be scraped by collimators to avoid hitting the superconducting magnets. Part of this beam could possibly be extracted by a crystal into a fixed-target experiment*.

In the extraction experiment, the SPS is operated at 120 GeV where a coasting beam of $5 \cdot 10^{11}$ protons has a lifetime in excess of one hundred hours. The normalised horizontal and vertical emittances are 6-8 mm·mrad for the unperturbed beam. Diffusion is created by exciting the beam horizontally with band-limited white noise. The crystal is placed 10 mm from the closed orbit and the horizontal beam emittance is around 60 mm·mrad when the large-amplitude particles reach the crystal. The typical impact parameters of the particles on

* At the time of writing, a collider experiment seems to be favoured over an experiment with a crystal-extracted beam.

the crystal are of the order of one micron. The layout of the SPS for crystal extraction is shown in Fig. 25.

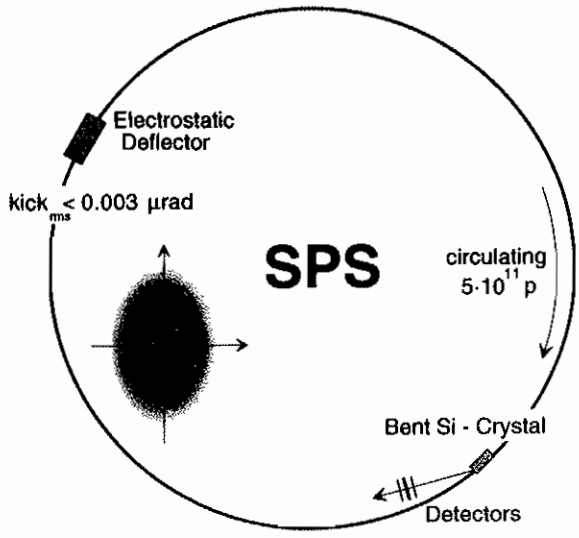

Fig. 25 Layout of SPS for crystal extraction

In the SPS experiment [43], 3-cm long (110) Si crystals, mounted in a U-shaped bending device, are used to extract the beam, like in Fig. 22 a). The benders are mounted on a goniometer to align the planar direction with the beam. The benders can furthermore be translated towards the circulating beam. The extraction angle is 8.5 mrad, and the crystals are prealigned and monitored by laser beams reflected from the polished surface of the crystals. The position of the essential elements in the extraction straight section are shown in Fig. 26, together with the crystal bending device. Several particle detectors allow observation of the extracted beam. We mention scintillators (S), scintillator hodoscopes (H), scintillating screens observed with a camera (TV) and position sensitive microstrip gas chambers (MSGC).

For prealigned crystals, extraction is easily obtained with efficiencies of up to 10%. This efficiency is determined from intensity monitors in the extracted beam and the beam lifetime in a steady-state diffusion mode. As discussed above, efficiencies up to 40% are theoretically possible.

The angular acceptance of the crystal has been measured by monitoring the extracted intensity as a function of planar angle to the beam, Fig. 27. The width of the distribution is much larger than expected, namely around 200 μrad to be compared to $2\psi_p$=28 μrad. Furthermore the observed beam profiles are for some orientations of the crystal wide and show double peaks. These observations can to some extent be explained by the so-called 'anticlastic' bending of the crystal in the bending device used. As seen on the inserts in Fig. 26, the crystal is also bent perpendicular to the direction of the bend. Furthermore, and more seriously, the planar direction varies with the vertical coordinate at the entrance of the crystal. Clearly a beam with a vertical size of more than 1 mm will produce an angular peak larger than $2\psi_p$ with a decreased extraction efficiency. Furthermore, multi-pass extraction may be involved in the explanation. A particle not channeled or dechanneled may stay in the machine even when it is multiple scattered from the 3 cm Si. The particle may then be extracted on subsequent passes of the crystal. Such multi-pass extraction has been discussed in [47,48].

The SPS extraction experiments are continuing in order to understand fully the observations. One improvement is the installation of a bent crystal without anticlastic bending,

namely a crystal cut in U-shape. This crystal is shown in Fig. 28.

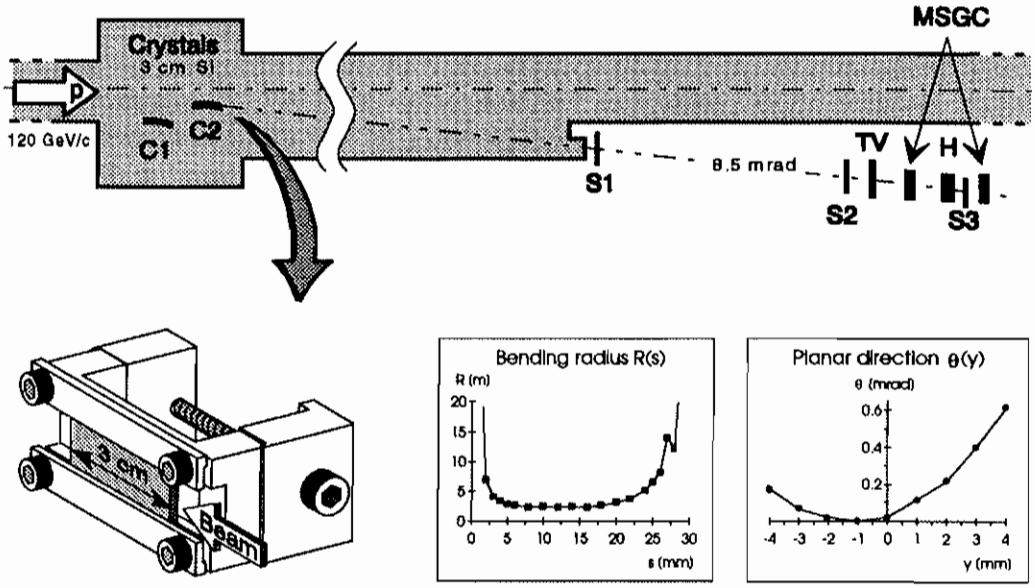

Fig. 26 Layout of straight section used for crystal extraction in SPS

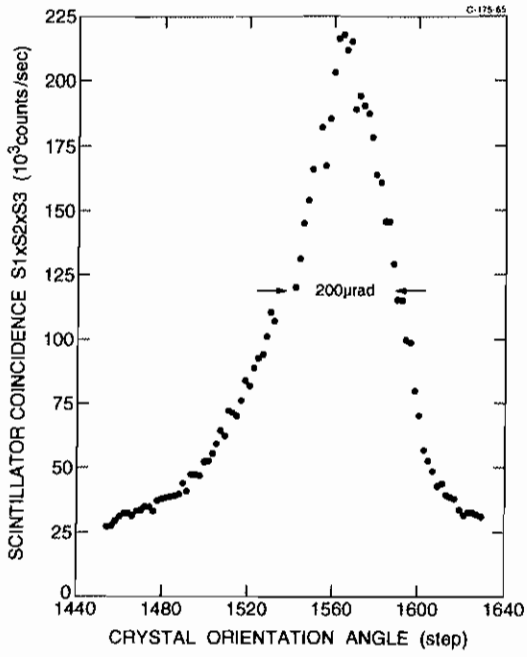

Fig. 27 Measured angular acceptance of extracting crystal

Furthermore it is very important to understand the influence of the crystal on the

machine itself, in particular what the crystal will do to the collimation of the machine. (A silicon crystal 3 cm. long represents 6 % of a nuclear interaction length.) This is important for the background in collider detectors, and also for the quench protection of the superconducting magnets.

Also the point of radiation damage has to be investigated in detail, in particular because the exposed area of an extracting crystal will be small owing to the small impact parameters. At fluences of 10^{19} protons/cm^2 no noticeable efficiency deterioration at 70 GeV has been seen at Serpukhov [49], whereas a deterioration of low-energy channeling has been observed by Baker et al. [50] for a crystal exposed to $4{\cdot}10^{20}$ protons/cm^2 at 28 GeV. It is, however, not evident how to relate this damage observed at low energy to high-energy dechanneling.

Finally, it is important to study crystal extraction at as high an energy as possible, in order to make a safe extrapolation to LHC energies. At the Tevatron, extraction tests are being prepared for 0.9 TeV [44].

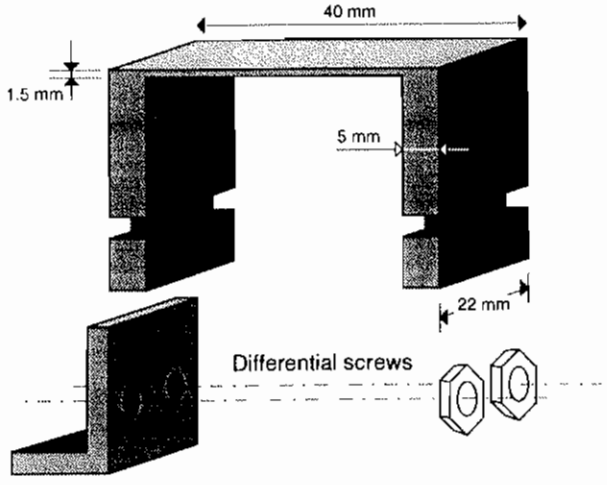

Fig. 28 Size of U-shaped crystal

8. CONCLUSIONS AND OUTLOOK

Channeling is today a well-founded effect occurring when charged particles are incident on single crystals in directions close to crystallographic directions.

The coherent scatterings on the strings or planes of atoms, which a crystal consists of, change dramatically the transmission of such channeled particles, in comparison to amorphous materials. This means that the channeling effect can be used to study fundamental processes in both atomic, nuclear and particle physics.

In particular, the strong steering effect can be applied in bending and focusing of beams replacing magnets with crystals. The bending powers are very large and the inherent losses acceptable. Efficiencies up to 50 % have been demonstrated.

Crystals are also potentially useful as extraction devices, in particular because of the inherently small septum thickness. Extraction with efficiencies up to 10 % have been

demonstrated.

The first real applications of crystals as beamline elements have been made, and the potential for other applications of the immense crystalline fields seems large. Especially applications at very high energies are promising because of the increasing dechanneling length and the slowly decreasing critical angles with energy.

Acknowledgements

The present lecture is an overview of the work done by a large number of scientists and technicians over a period of almost twenty years. Without the enormous effort by all these people, our knowledge about channeling, and in particular at high energy, would not have advanced this far.

REFERENCES

[1] O. Fich et al., Phys. Lett. 57B (1975) 90.

[2] G.R. Piercy, F. Brown, J.A. Davies and M. McCargo, Phys. Rev. Lett. 10 (1963) 399.

[3] R.S. Nelson and M.W. Thomson, Phil. Mag. 8 (1963) 1677.

[4] M.T. Robinson and O.S. Oen, Appl. Phys. Lett. 2 (1963) 3032; Phys. Rev. 132 (1963) 2385.

[5] J. Lindhard, Kgl. Danske Videnskab. Selskab, Mat. Fys. Medd. 34 (1965) No.14; Phys. Lett. 12 (1964) 126.

[6] J. Stark, Physik. Zeitsch. 13 (1912) 973.

[7] A.A. Vorobiev, V.V. Kaplin and S.A. Vorobiev, Nucl. Instrum. Methods 127 (1975) 265.

[8] M.A. Kumakhov, Phys. Lett. 57 (1976) 17.

[9] R.L. Swent et al., Phys. Rev. Lett. 43 (1979) 1723.

[10] J.U. Andersen and E. Lægsgård, Phys. Rev. Lett. 44 (1980) 1079.

[11] E.N. Tsyganov, Fermilab TM-682, TM-684, Batavia, (1976) (unpublished).

[12] A.F. Elishev et al., Phys. Lett. 88B (1979) 387.

[13] J. Bak et al., Phys. Lett. 93B (1980) 505.

[14] N. Bohr, Kgl. Videnskab. Selskab, Mat. Fys. Medd. 18 (1948), nr. 8.

[15] J.S. Forster et al., Nucl. Phys. B318 (1989) 301, and R.A. Carrigan in Relativistic Channeling, R.A. Carrigan and J.A. Ellison (eds.), (NATO ASI series Vol. B 165, 1987).

[16] V.M. Biruykov et al., submitted to Nucl. Instrum. Methods in Phys. Research.

[17] J.F. Bak et al., Nucl. Phys. B242 (1984) 1.

[18] C.R. Sun et al., Nucl. Instr. and Meth. B2 (1984) 60.

[19] J.F. Bak et al., Nucl. Phys. A 389 (1982) 533.

[20] S.K. Andersen et al., Nucl. Phys. B 167 (1980) 1.

[21] J.F. Bak et al., Phys. Rev. A 25 (1982) 1334.

[22] H. Esbensen et al., Phys. Rev. B 18 (1978) 1039.

[23] J. Bak et al., Nucl. Phys. B 254 (1985) 491.

[24] R. Medenwaldt et al., Phys. Lett. B 242 (1990) 517.

[25] R. Medenwaldt et al., Phys. Lett. B 281 (1992) 153.

[26] J.F. Bak et al., Phys. Lett. B 202 (1988) 615.

[27] R. Medenwaldt et al., Phys. Lett. B 227 (1989) 483.

[28] H. Kudo, Nucl. Instrum. Meth. 189 (1981) 609.

[29] J.A. Ellison, Nucl. Phys. B206 (1982) 205.

[30] S.I. Baker, Nucl. Instrum. Methods in Phys. Res. A248 (1986) 301.

[31] L.I. Bel'zer et al., JETP Lett. 46 (1987) 381.

[32] S.I. Baker et al., Phys. Lett. 137B (1984) 129.

[33] V.A. Andreev et al., JETP. Lett. 36 (1982) 415.

[34] S.P. Møller et al., Phys. Lett. B256 (1991) 91.

[35] S.P. Møller et al., Nucl. Instrum. Methods in Phys. Res. B84 (1994) 434.

[36] M. Clement et al., CERN/SL/92-21, 1992 (unpublished).

[37] A.S. Denisov et al., Nucl. Instrum. Methods in Phys. Res. B69 (1992) 382.

[38] V.A. Andreev et al., JETP. Lett. 41 (1985) 408.

[39] G.D. Barr et al., CERN/SPSC/90-22, SPSC/P253 (experiment NA48), 1990 (unpublished).

[40] D. Chen et al., Phys.Rev.Lett. 69 (1992) 3286.

[41] V.V. Avdeichikov et al., JINR Communication 1-84, Dubna (1984) [English translation: Fermilab 80/45 (1980)], unpublished.

[42] A.A. Asseev et al., Nucl. Instrum. Methods in Phys. Res., A334 (1993) 283, and references therein.

[43] H. Akbari et al., Phys. Lett. B313 (1993) 491.

[44] R.A. Carrigan et al., Nucl. Instrum. Methods in Phys. Res. B90 (1994) 128.

[45] M. Gyr, private communication.

[46] RD 22 Collab., B.N. Jensen et al., CERN/DRDC 91-25, DRDC/P29 (unpublished), and K. Kirsebom et al., CERN/LHCC/93-45, LHCC/I5 (unpublished).

[47] V.M. Biruykov, Nucl. Instrum. Methods B53 (1991) 202.

[48] A.M. Taratin et al., Nucl. Instrum. Methods B58 (1991) 103.

[49] Yu.A. Chesnokov et al., Proc. of the XV Int. Conf. on High Energy Accelerators (Hamburg, 1992).

[50] S. Baker et al., Nucl. Instrum. Methods in Phys. Res. B90 (1994) 119.

BIBLIOGRAPHY

D.S. Gemmell, Channeling and related effects in the motion of charged particles through crystals, Rev. Mod. Phys 46 (1974) 129.

D.V. Morgan, Channeling (J. Wiley and Sons, London, 1973).

L.C. Feldman, J.W. Mayer and S.T. Picraux, Materials Analysis by Ion Channeling (Academic Press, London, 1982).

Y. Ohtsuki, Charged Beam Interaction with Solids, (Taylor and Francis, Ltd., 1983).

R.A. Carrigan and J.A. Ellison (eds.), Relativistic Channeling, (NATO ASI series Vol. B 165, (1987).

A.H. Sørensen and E. Uggerhøj, Channeling, Radiation and Applications, Nuclear Science Applications 3 (1989) 147.

V.N. Baier et al., Pair Creation by a Photon in Oriented Single Crystals, Nuclear Science Applications 3 (1989) 245.

S.P. Møller, Energy-Loss Distributions of High-Energy Particles Traversing Thin Si and Ge Crystals, Nuclear Science Applications 3 (1989) 259.